



# Spectroscopic and theoretical optical properties of indoleninyl-substituted dibenzotetraaza[14]annulenes

Abdul Qaiyum Ramle <sup>a</sup>\*, Asli Karakas <sup>b</sup>\*\*, Abdul Kariem Mohd. Arof <sup>c</sup>, Mustafa Karakaya <sup>d</sup>,  
Mehmet Taser <sup>b</sup>, Aysun Gozutok <sup>b</sup>, Chee Chin Fei <sup>e</sup>, Nurhidayatullaili Muhd. Julkapli <sup>e</sup>, Wan  
Jefrey Basirun <sup>a</sup>\*\*\*

<sup>a</sup> Department of Chemistry, University of Malaya, 50603 Kuala Lumpur, Malaysia.

<sup>b</sup> Department of Physics, Faculty of Sciences, Selcuk University, 42049 Campus, Konya, Turkey.

<sup>c</sup> Department of Physics, University of Malaya, 50603 Kuala Lumpur, Malaysia.

<sup>d</sup> Department of Energy Systems, Faculty of Engineering & Architecture, Sinop University, 57000 Sinop, Turkey.

<sup>e</sup> Nanotechnology & Catalysis Research Centre (NanoCat), Institute of Postgraduate Studies, 50603, Kuala Lumpur, Malaysia.

Corresponding authors: [qaiyum@um.edu.my](mailto:qaiyum@um.edu.my). \* (A. Q. Ramle),

[akarakas@selcuk.edu.tr](mailto:akarakas@selcuk.edu.tr). \*\* (A. Karakas)

[jeff@um.edu.my](mailto:jeff@um.edu.my). \*\*\* (W. J. Basirun)

This article has been accepted for publication and undergone full peer review but has not been through the copyediting, typesetting, pagination and proofreading process which may lead to differences between this version and the Version of Record. Please cite this article as doi: 10.1002/jhet.4074

### Abstract

Two new macrocyclic dibenzotetraaza[14]annulene (DBTAA) compounds with indolenine (**5**) and pyridoindolenine (**6**) moieties were synthesized and characterized by spectroscopy. Both DBTAAs exhibit strong UV-Vis absorption properties in the Soret band region. The theoretical second-order non-linear optical (NLO) property, electric dipole moment ( $\mu$ ), dispersion-free dipole polarizability ( $\alpha$ ) and first hyper-polarizability values were calculated by density functional theory (DFT) and time dependent density functional theory (TDDFT). The *ab-initio* quantum mechanical calculation by time-dependent Hartree-Fock (TDHF) method was utilized to investigate the dynamic dipole polarizabilities, dynamic second-order, static and dynamic third-order ( $\gamma$ ) hyper-polarizabilities of the DBTAAs. The configuration interaction (CI) technique of all doubly occupied molecular orbitals (MOs) possesses theoretically defined single-photon absorption (OPA) specifications for the examined structures. The computed maximum OPA wavelengths on both macrocyclic compounds coincide with the preceding measurement outcomes.

**Keywords:** DBTAA; UV-Visible; Polarizability; Hyper-polarizability; DFT.

## 1. Introduction

Macrocyclic compounds based on porphyrin structures as optical materials have been widely explored and applied in important applications for the past few decades.<sup>[1,2]</sup> However a similar analogue of porphyrin, the dibenzotetraaza[14]annulene (DBTAA) is seldom reported and studied. Both structures consist of four nitrogen atoms in the inner ring which are easily coordinated with a metal cation to form the metal complex.<sup>[3,4]</sup> DBTAA is classified as a Hückel anti-aromatic ( $4n$ ) compound.<sup>[5,6]</sup> In contrast, the porphyrin molecule is a Hückel aromatic ( $4n+2$ ) with the  $\pi$ -electrons fully conjugated through the entire ring.<sup>[7,8]</sup> The geometry of DBTAA is more flexible compared to the porphyrin, where the structure possesses a saddle-shaped conformation with the introduction of a methyl group at the 1 and 3 positions of the propanediiminato moiety.<sup>[9,10]</sup> Besides, the DBTAA is easily synthesized by a simple [2+2] Schiff base condensation reaction between a 1, 3-dicarbonyl and *o*-phenylene diamine reactants.<sup>[11]</sup> However, changing the substituent at the *meso*-position of the DBTAA molecule is quite challenging due to the limited synthetic possibilities.

The fundamental design of organic non-linear optical (NLO) structures is built on the  $\pi$ -bond order in view of the overlapping effect of the  $\pi$ -orbital delocalization from the electronic charge dispersion.<sup>[12-14]</sup> The presence of electron-donor or acceptor substituents in the molecular structure could promote the asymmetric electronic dispersion and consequently improve the NLO properties.<sup>[15-17]</sup> The quadratic NLO properties of organic compounds have been widely

investigated due to their advantages in the synthesis of materials.<sup>[18-20]</sup> However, only few delocalized  $\pi$ -electron systems with low optical transparencies could be utilized in useful applications such as optical wave guides and second-harmonic generators.<sup>[21]</sup> Furthermore, efficient optical transmittance at the UV-Vis region is particularly preferable in a NLO crystal. In addition to the linear optical and second-order NLO effects, the third-order optical nonlinearity gathers some interest.<sup>[22,23]</sup> The third-order NLO systems have important applications such as third-harmonic generators (THG) and are optical limiting.<sup>[24,25]</sup> The dipole and quadrupole moments and the hyper-polarizability could be calculated by means of *ab-initio* computations using logically high correlation levels and suitable basis sets.<sup>[26,27]</sup>

The DBTAA has promising NLO behavior and might possess very interesting second and third-order NLO properties. The NLO phenomena of the compounds could be preliminarily assessed *via* theoretical methodologies. The DFT and TDHF methodologies were performed on the two DBTAA compounds to predict the second and third-order NLO responses of the molecules. The theoretical computations of the linear optical, quadratic and cubic NLO responses could provide accurate data for the synthesis of new and efficient DBTAA compounds. Thus the objective of this work is to define the effects of microscopic second-order and third-order optical nonlinearities of the DBTAA moieties. Apart from the NLO properties, the HOMO-LUMO energies and energy band gaps of the first and second frontier MOs and the electronic transition wavelengths belonging to the lowest lying electronic transitions were attained by computational methods using the DFT/B3LYP and CI processes, respectively. The calculation results on the OPA wavelength were compared with the experimental results from UV-Vis spectroscopy. The experimental details of the synthesis and characterization methods are described in the electronic supporting information (ESI).

## 2. Computational studies

Computational studies include the assignment of electric dipole moments and tensor components of static dipole polarizability and the first hyper-polarizability. Geometrical optimizations were implemented on the DBTAA **5** and **6**. The electric dipole moments, dispersion-free dipole polarizabilities and the first hyper-polarizabilities were calculated after generating the geometrical optimizations. The finite field (FF) method was used to calculate the  $\mu$ , static  $\alpha$  and  $\beta$  values.<sup>[28]</sup> The FF scheme introduces an apprehensible approach to the computation of the hyper-polarizability values.<sup>[29]</sup> To achieve a certain polarizability and hyper-polarizability level, the 6-31G(*d*) polarized basis set was used in this work and the results were satisfactory. It is expected that this basis set could reveal the molecular structures in the near Hartree-Fock standard. The GAUSSIAN03W<sup>[30]</sup> program at the DFT/ B3LYP level with 6-31G(*d*) polarized basis set were used to execute the geometrical optimizations,  $\mu$ , static  $\alpha$  and  $\beta$  computations. The GaussView program was used as the interface program for the GAUSSIAN03W in order to design the molecular models for both the macrocyclic DBTAA compounds. The performance of the DFT techniques in the calculation of the electro-optical properties were investigated systematically in the literature.<sup>[31]</sup> The hyper-polarizability tensor components of the organic and organometallic materials are extensively derived by means of the B3LYP function.<sup>[32,33]</sup> It is known that the subject functional generates the logical experimental

trends.<sup>[34,35]</sup> The calculated averaged orientation (isotropic) dipole polarizability  $\langle\alpha\rangle$  and the  $\beta_{\text{tot}}$  (total first static hyper-polarizability) are as follows:<sup>[36]</sup>

$$\langle\alpha\rangle = (\alpha_{xx} + \alpha_{yy} + \alpha_{zz}) / 3 \quad (1)$$

$$\beta_{\text{tot}} = [(\beta_{xxx} + \beta_{xyy} + \beta_{xzz})^2 + (\beta_{yyy} + \beta_{xzz} + \beta_{yxx})^2 + (\beta_{zzz} + \beta_{zxx} + \beta_{zyy})^2]^{1/2} \quad (2)$$

Computational methodologies are theoretical means for the calculation of hyper-polarizabilities. The self-consistent field technique of the TDHF often generates the frequency-dependent hyper-polarizability values.<sup>[26]</sup> The  $\gamma(0;0,0,0)$  at  $\omega = 0$  and  $\alpha(-\omega;\omega)$ ,  $\beta(-2\omega; \omega, \omega)$ ,  $\gamma(-3\omega; \omega, \omega, \omega)$  computations at  $\omega = 0.04282$  atomic units (a.u.) (1064 nm) were achieved by the TDHF method with the 6-31G(d) basis set executed in the GAMESS<sup>[37]</sup> program. The static third-order hyper-polarizabilities are represented by  $\gamma(0;0,0,0)$  as stated above. The second-harmonic generation (SHG) and THG groups in the TDHF method were utilized in the calculations of the  $\beta(-2\omega; \omega, \omega)$  and  $\gamma(-3\omega; \omega, \omega, \omega)$ , respectively, at  $\omega$  frequencies. The computations of dynamic quadratic hyper-polarizabilities are frequently characterized by the style of  $\beta - V$  ( $\beta$  vector) which indicates the vectorial portion of the second-order hyper-polarizability. The following equations were used to calculate the  $\beta - V$  and averaged (isotropic) cubic hyper-polarizabilities  $\langle\gamma\rangle$

$$\beta - V = (\beta_x^2 + \beta_y^2 + \beta_z^2)^{1/2} \quad (3)$$

where  $\beta_i (i = x, y, z)$  is designed by:

$$\beta_i = (1/3) \sum_{j=x,y,z} (\beta_{ijj} + \beta_{jij} + \beta_{jji}) \quad (4)$$

$$\langle\gamma\rangle = (1/5)[\gamma_{xxx} + \gamma_{yyy} + \gamma_{zzz} + 2(\gamma_{xyy} + \gamma_{xxz} + \gamma_{yyz})] \quad (5)$$

The transition wavelength  $\lambda_{\max}$  with the lowest lying electronic transitions are indicated using the CIDRT approach (configuration interaction including all doubly occupied MOs from the Hartree-Fock reference determinant) of the TDHF procedure with 6-31G basis set executed in the GAMESS program. Calculations of the dynamic dipole polarizabilities, hyper-polarizabilities and maximum OPA wavelengths were accomplished on a PC with an Intel (R) core (TM) I7-2630QM operator, 5.8 GB RAM memory and 2 GHz frequency using Linux PC GAMESS version running under Linux Fedora release 11 (Leonidas) environment. Besides, to perceive the relevancy between the molecular structures and NLO behavior; the HOMOs, LUMOs and HOMO-LUMO energy band gaps were derived from the GAUSSIAN03W program at the TD-DFT/ B3LYP level utilizing the 6-31G(*d*) basis set. The energy band gap value of  $E_g$  for the first and second frontier MOs is formulated as follows:

$$E_g = E_{\text{LUMO}} - E_{\text{HOMO}} \quad (6)$$

### 3. Results and discussions

#### 3.1 Synthesis and characterizations

Scheme 1 shows that compounds **1**<sup>[38]</sup>, **3** and **4**<sup>[39]</sup> were synthesized according to the literature. The reduction of **1** was catalyzed by SnCl<sub>2</sub>·2H<sub>2</sub>O in acidic media to produce diamine **2** in moderate yields. Subsequently, the crude diamine was used for the [2+2] condensation reaction with diformyl **3** or **4**, affording the desired macrocyclic DBTAA **5** or **6** in good yields. The formation of macrocycle was achieved through the migration of double bonds from the pyrrole ring to the annulene ring.<sup>[40]</sup> Additionally, the presence of linear octyloxyl group on the dibenzo moiety enhances the solubility of the macrocycles in polar organic solvents of CH<sub>3</sub>Cl,

CH<sub>2</sub>Cl<sub>2</sub>, THF, acetic acid and pyridine. However, both compounds were insoluble in non-polar hydrocarbons and alcoholic solvents.

<Scheme 1>

The structures of both macrocyclic compounds were confirmed by NMR spectroscopy, where the two N-H ring protons of **5** and **6** appear as a triplet signal with similar  $J = 6.4$  Hz at  $\delta$  14.96 and 15.10 ppm, respectively. Similarly, the four olefinic (N=CH) protons of **5** and **6** emerge as a doublet signal due to the coupling with the N-H ring protons, which is clearly observed at  $\delta$  values of 8.71 ppm ( $J = 6.0$  Hz) and 8.92 ppm ( $J = 5.6$  Hz), respectively. These results confirm that the N-H ring exhibits the imine-enamine tautomerism conformation in the solution, consistent with previous reports.<sup>[41, 42]</sup> The FT-IR analysis of Fig. S11 and S12 (ESI), indicate that the N-H vibration signals of the inner ring are not clearly observed at *ca.* 3300 cm<sup>-1</sup>. This is due to the N-H...N intramolecular H-bonding interactions on the 1, 3-propanediiminato fragments. Moreover, the presence of strong stretching bands at 1633 cm<sup>-1</sup> and 1632 cm<sup>-1</sup> are assigned to the C=N annulene rings of **5** and **6**, respectively. The two intense absorption bands at 1248-1249 and 1182-1184 cm<sup>-1</sup> ranges are correlated with the C-O-C stretching mode in the dibenzo unit. Finally, the combination of the NMR and FT-IR spectroscopic results are in good agreement with the proposed structures.

### 3.2 UV-Vis absorption spectra

The UV-Vis absorption spectra for both macrocycles were recorded in CHCl<sub>3</sub> solution (5  $\mu$ M concentration) between 300 nm to 650 nm and the electronic parameters are tabulated in Table 1. As shown in Fig. 1, the most intense absorption Soret band for **5** is observed at 395 nm

with a molar absorption coefficient,  $\epsilon = 0.758 \times 10^5 \text{ M}^{-1} \text{ cm}^{-1}$ . This spectrum displays a slight bathochromic shift (*ca.* = 18 nm) in the presence of the electron donating octyloxy group compared to the core indolenine-DBTAA structure.<sup>[43]</sup> Furthermore, the spectrum of **6** exhibits a bathochromic shift (*ca.* = 22 nm) compared to **5**, due to extension of the  $\pi$  – conjugation system. As a result, the HOMO-LUMO energy gap decreases by 0.063 eV. The most intense absorption band of both macrocycles are assigned to the  $\pi$ - $\pi^*$  transition in the macrocyclic DBTAA moiety,<sup>[44,45]</sup> whereas the weak absorption band at 339 nm of **6** is assigned to the  $\pi$ - $\pi^*$  transition of the pyridoindolenine moiety. The calculated full-half width maximum (FWHM) of **6** is broader than **5**, indicating a strong absorption of light with a wide wavelength range.

<Figure 1>

<Table 1>

### 3.3 Theoretical calculations

The geometrically optimized structures of **5** and **6** in Fig. S13 (ESI) were calculated by the DFT/B3LYP method. The results show that both DBTAA structures are planar shaped and closely resembles the crystallographic data as tabulated in Table S1 (ESI).<sup>[46]</sup> Moreover, to gain some insight on the molecular orbital structures, the HOMO and LUMO energies for both macrocycles have been examined and their electronic properties are presented in Table 2. As shown in Fig. 2, the electron density of LUMOs of both DBTAAs are delocalized over the entire annulene ring only, while the HOMOs are distributed around the indolenine and annulene ring. Interestingly, the electron cloud of **6** at the LUMO+1 is clearly shifted to both sides of the pyridoindolenine group as an extension of the  $\pi$ -conjugation in the structure. Unlike **5**, the

electron cloud did not change significantly compared to the LUMO. Moreover, the presence of pyridoindolenine in the macrocyclic framework decreases the HOMO-LUMO gap of **6** by 0.05 eV compared to **5**. This is due to the tuning of energy levels and the extension of the  $\pi$  – conjugated system.

The electronic transitions of both macrocycles were calculated and the absorption wavelength, oscillator strength and major contributions are presented in Table 3. Macrocycles **5** and **6** possess an intense simulated major absorption peak centered at  $\lambda_{\text{max}} = 409.4$  nm and 429.0 nm with a relatively high oscillator strength,  $f = 0.9150$  and 0.8008, respectively. However, the two calculated additional peaks of **5** at 486.8 nm and 620.5 nm, and **6** at 631.0 nm are absent in the spectrum due to the extremely low  $f$  values. Furthermore, the simulated spectrum of **6** also displays a bathochromic shift (*ca.* 20 nm) compared to **5**, and is close to the experimental result depicted in Fig. 1.

<Figure 2>

<Table 2>

<Table 3>

Table 4 shows the electric dipole moments of **5** and **6**. As reported by Di Bella *et al.*, the computed ground level electric dipole moment of a tetraazamacrocyle ligand was 2.2 D by using the INDO/S-SOS formalism.<sup>[47]</sup> In comparison, we found that the  $\mu$  value is roughly 1.3 and 2.7 times higher than the calculated data for **5** and **6**, respectively. The differences in these values could be due to the better  $\pi$ -electrons delocalization over the planar macrocycle. On the other hand, the  $\mu$  value of **6** is smaller than **5** which is attributed to the electron-donating effect of the pyridoindolenine group.

<Table 4>

The dispersion-free dipole polarizabilities, the second and third-order hyper-polarizabilities data are tabulated in Table 5-7, respectively. As can be observed, the theoretical results of static  $\langle\alpha\rangle$ ,  $\beta_{\text{tot}}$  and  $\langle\gamma\rangle$  shows a decrease in **5** compared to **6**. Compared to the published literature, the calculated values of  $\beta_{\text{tot}}$  for **5** and **6** are 9.6 and 15.5 times higher compared to the tetraazamacrocyle ligand ( $\beta = 4.3 \times 10^{-30}$  esu), respectively.<sup>[47]</sup> This is because both DBTAAs possess better charge transfer character due to the electron rich structures. Also, the decrease of the HOMO-LUMO energy gap from the effect of the substituent groups might contribute to a higher  $\beta_{\text{tot}}$  value.<sup>[48,49]</sup> Interestingly, **6** has a larger  $\beta_{\text{tot}}$  value compared to experimental values of various substituted metal free phthalocyanines ( $\beta = 25.1 - 44.9 \times 10^{-30}$  esu).<sup>[50]</sup> Hence, **6** could be useful for NLO applications.

<Table 5>

<Table 6>

<Table 7>

Generally, the quadratic and cubic hyper-polarizability parameters strongly influence the electro-optical coefficients. Both are dependent on the shape and size of the material and electron delocalization around the charge transfer transmission. The NLO parameters are also affected by the optical field frequencies. As shown in Table 8-10, the magnitudes of the frequency-dependent dipole polarizabilities, second and third-order hyper-polarizabilities of **5** are lower than **6**. This indicates an identical decrease with the static ones. The involvement of the  $\pi -$

conjugated pyridoindolenine group enhances the static and dynamic  $\langle\alpha\rangle$ ,  $\beta_{\text{tot}}$ ,  $\beta - V$ , and  $\langle\gamma\rangle$  values of **6** compared to **5** (Table 5-10). Thus, an increase in the second and third-order NLO properties of **6** is observed. The cubic hyper-polarizability,  $\langle\gamma\rangle$  value of **6** is twice larger compared to **5**, which confirms that the introduction of a  $\pi$  - conjugated group in the DBTAA structure increases the magnitude and molecular dipole moment parameter, which consequently improves the NLO properties.<sup>[51]</sup>

<Table 8>

<Table 9>

<Table 10>

#### 4. Conclusions

In summary, two new DBTAAs were synthesized in good yields and successfully characterized by NMR, IR and UV-Vis. The geometry of both DBTAAs were optimized by the DFT method which suggests a planar structure. The simulated UV-Vis spectra and the calculated HOMO-LUMO band gap for both DBTAAs matches well with the experimental results. DBTAA **6** exhibits higher static and dynamic  $\beta_{\text{tot}}$ ,  $\beta - V$ ,  $\langle\gamma\rangle$  values and thereby possesses better second and third-order NLO properties compared to DBTAA **5**. For future work, the experimental and computational designs *via* structural modification of the DBTAA structures are needed to improve NLO properties, as well as to discover the potential NLO applications.

#### 5. Acknowledgements

This work is supported by Ministry of Higher Education, Malaysia (Grants: ST027-2019 and ST011-2019). The authors declare that there is not conflict of interest.

## 6. References

- [1] A. Ambroise, R.W. Wagner, P.D. Rao, J.A. Riggs, P. Hascoat, J.R. Diers et al. *Chem. Mater.* 2001, 13, 1023.
- [2] A. Mahmood, J.-Y. Hu, B. Xiao, A. Tang, X. Wang, E. Zhou, *J. Mater. Chem. A* 2018, 6, 16769.
- [3] H. Khaledi, M.M. Olmstead, T. Fukuda, H. Mohd Ali, *Inorg. Chem.* 2014, 53, 11348.
- [4] Z. Liang, M. Damjanović, M. Kamila, G. Cosquer, B.K. Breedlove, M. Enders et al. *Inorg. Chem.* 2017, 56, 6512.
- [5] K.M. Zwoliński, J. Eilmes, *Chem. Commun.* 2016, 52, 4084.
- [6] A.M. Whyte, Y. Shuku, G.S. Nichol, M.M. Matsushita, K. Awaga, N. Robertson, *J. Mater. Chem.* 2012, 22, 17967.
- [7] S. Dey, J.R. Dewey, B.B. Wayland, M.J. Zdilla, *New J. Chem.* 2018, 42, 19369.

- [8] V.L. Goedken, J.J. Pluth, S.-M. Peng, B. Bursten, *J. Am. Chem. Soc.* 1976, 98, 8014.
- [9] P. Mountford, *Chem. Soc. Rev.* 1998, 27, 105.
- [10] M.D. Walter, R. Fandos, R.A. Andersen, *New J. Chem.* 2006, 30, 1065.
- [11] A.Q. Ramle, H. Khaledi, A.H. Hashim, M.A. Mingsukang, A.K. Mohd Arof, H.M. Ali et al. *Dyes Pigm.* 2019, 164, 112.
- [12] D.S. Chemla, J. Zyss, In: D.S. Chemla, J. Zyss (eds.). *Nonlinear Optical Properties of Organic Molecules and Crystals*. Academic Press, New York, 1987, Ch. II-1 pp. 54-139.
- [13] C.H. Bosshard, M. Bösch, I. Liakatas, M. Jäger, P. Günter, In: P. Günter (ed.). *Nonlinear Optical Effects and Materials*. Springer-Verlag, Berlin, 2000, Ch. 3 pp. 163-166.
- [14] M. Jazbinsek, O.P. Kwon, Ch. Bosshard, P. Günter, In: S.H. Nalwa (ed.). *Handbook of Organic Electronics and Photonics*. American Scientific Publishers, Los Angeles, 2008 [chapter 1]
- [15] H.O. Marcy, M.J. Rosker, L.F. Warren, P.H. Cunningham, C.A. Thomas, L.A. DeLoach et al. *Opt. Lett.* 1995, 20, 252.

- [16] H.W. Zhang, A.K. Batra, R.B. Lal, *J. Cryst Growth* 1994, 137, 141.
- [17] C.C. Frazier, M.P. Cockerham, E.A. Chauchard, C.H. Lee, *J. Opt. Soc. Am. B.* 1987, 4, 1899.
- [18] B. J. Coe, D. Beljonne, H. Vogel, J. Garín, J. Orduna, *J. Phys. Chem. A* 2005, 109, 10052.
- [19] P.N. Prasad, D.J. Williams, *Introduction to Nonlinear Optical Effects in Organic Molecules and Polymers*. Wiley, New York, USA, 1991, Ch. 1 pp 1-6.
- [20] S.R. Marder, B. Kippelen, A.K.Y. Jen, N. Peyghambarian, *Nature* 1997, 388, 845.
- [21] S.G. Prabhu, P. Mohan Rao, S.I. Bhat, V. Upadyaya, S.R. Inamdar, *J. Cryst. Growth* 2001, 233, 375.
- [22] B. Sahraoui, G. Rivoire, N. Terkia-Derdra, M. Sallé, J. Zarembo, *J. Opt. Soc. Am. B* 1998, 15, 923.
- [23] A. Zawadzka, A. Karakas, P. Płóciennik, J. Szatkowski, Z. Lukasiak et al. *Dyes Pigm.* 2015, 112, 116.
- [24] J.S. Shirk, R.G.S. Pong, F.J. Bartoli, A.W. Snow, *Appl. Phys. Lett.* 1993, 63, 1880.

- [25] A. Bhardwaj, P.O. Hedekvist, K. Vahala, *J. Opt. Soc. Am. B.* 2001, 18, 657.
- [26] D.P. Shelton, J.E. Rice, *Chem. Rev.* 1994, 94, 3.
- [27] G. Maroulis, *Chem. Phys. Lett.* 1998, 289, 403.
- [28] H.A. Kurtz, J.J.P. Stewart, K.M. Dieter, *J. Comput. Chem.* 1990, 11, 82.
- [29] H.D. Cohen, C.C.J. Roothaan, *J. Chem. Phys.* 1965, 43, S34.
- [30] M.J. Frisch, G.W. Trucks, H.B. Schlegel, G.E. Scuseria, M.A. Robb et al. *Gaussian 03, Revision C.02*, Gaussian 03 (Gaussian Inc. Wallingford, CT), 2004.
- [31] G. te Velde, F.M. Bickelhaupt, E.J. Baerends, C. Fonseca Guerra, S.J.A. van Gisbergen et al. *J. Comput. Chem.* 2001, 22, 931.
- [32] I.C. de Silva, R.M. de Silva, K.M. Nalin de Silva, *J. Mol. Struct: THEOCHEM* 2005, 728, 141.
- [33] C. Mang, K. Wu, *Int. J. Quantum Chem.* 2006, 106, 2529.
- [34] P.L. Franzen, S.C. Zilio, A.E.H. Machado, J.M. Madurro, A.G. Brito-Madurro et al. *J. Mol. Struct.* 2008, 892, 254.

- [35] C. Cardoso, P.E. Abreu, F. Nogueira, *J. Chem. Theory Comput.* 2009, 5, 850.
- [36] K.S. Thanthiriwatte, K.M. Nalin de Silva, *J. Mol. Struct: THEOCHEM* 2002, 617, 169.
- [37] M.W. Schmidt, K.K. Baldrige, J.A. Boatz, S.T. Elbert, M.S. Gordon et al. *J. Comput. Chem.* 1993, 14, 1347.
- [38] S. Göker, G. Hızalan, Y.A. Udum, L. Toppare, *Synth. Met.* 2014, 191, 19.
- [39] A. Afghan, L. Roohi, M.M. Baradarani, J.A. Joule, *J. Heterocyclic Chem.* 2014, 51, 706.
- [40] F.L. Faraj, H. Khaledi, Y. Morimoto, S. Itoh, M.M. Olmstead, H.M. Ali, *Eur. J. Inorg. Chem.* 2014, 2014, 5752.
- [41] C.L. Honeybourne, *Tetrahedron Lett.* 1974, 15, 3075.
- [42] Ł. Dudek, J. Grolik, A. Kaźmierska, E. Szneler, A. Eilmes, K. Stadnicka, et al. *Tetrahedron Lett.* 2011, 52, 3597.
- [43] H. Rabaâ, H. Khaledi, M.M. Olmstead, D. Sundholm, *J. Phys. Chem. A* 2015, 119, 5189.
- [44] K.M. Zwoliński, L. Sieroń, J. Eilmes, *Org. Chem. Front.* 2018, 5, 171.

- [45] K.M. Zwoliński, J. Eilmes, *Org. Biomol. Chem.* 2018, 16, 5508.
- [46] H. Khaledi, M.M. Olmstead, H. Mohd Ali, N.F. Thomas, *Inorg. Chem.* 2013, 52, 1926.
- [47] S. Di Bella, I. Fragalà, *Eur. J. Inorg. Chem.* 2003, 2003, 2606.
- [48] Z. Liu, S. Hua, X. Yan, *J. Phys. Chem. A* 2018, 122, 2344.
- [49] N. Kumar, M. Paramasivam, J. Kumar, A. Gusain, P.K. Hota, *Spectrochim. Acta A* 2019, 206, 396.
- [50] G. Rojo, G. de la Torre, J. García-Ruiz, I. Ledoux, T. Torres, J. Zyss et al. *Chem. Phys.* 1999, 245, 27.
- [51] G. de la Torre, P. Vázquez, F. Agulló-López, T. Torres, *Chem. Rev.* 2004, 104, 3723.

### Figure and table captions

**Scheme 1:** Synthetic routes of DBTAA **5** and **6**. Reagents and conditions: (i) 1) EtOH, 37% HCl, SnCl<sub>2</sub>·2H<sub>2</sub>O, 70 °C, N<sub>2</sub>, 16 h. 2) 4 M NaOH.; (ii) EtOH, AcOH, reflux, N<sub>2</sub>, 6 h.

**Figure 1:** Experimental UV-Vis absorption spectra of **5** and **6** measured in CHCl<sub>3</sub> solution. The solid and dashed lines indicate the main experimental and simulation absorption peaks, respectively.

**Figure 2:** The frontier MOs of **5** and **6** calculated by DFT.

**Table 1:** Electronic parameters of **5** and **6**.

**Table 2:** Calculated first HOMO, LUMO and second HOMO-1, LUMO+1 frontier MO energies and  $E_g$  for **5** and **6** using DFT method at B3LYP/6-31G(*d*) level.

**Table 3:** Calculated absorption wavelengths, oscillator strengths and major compositions in terms of MO contributions for **5** and **6**.

**Table 4:** Calculated electric dipole moments,  $\mu$  (Debye) and dipole moment components for **5** and **6** using DFT method at B3LYP/6-31G(*d*) level.

**Table 5:** Selected components of the static  $\alpha(0;0)$  and  $\langle\alpha\rangle(0;0)$  ( $10^{-24}$  esu) values for **5** and **6** computed by DFT method at B3LYP/6-31G(*d*) level.

**Table 6:** Selected components of the static  $\beta(0;0,0)$  and  $\beta_{\text{tot}}(0;0,0)$  ( $10^{-30}$  esu) values for **5** and **6** computed by DFT method at B3LYP/6-31G(*d*) level.

**Table 7:** All static  $\gamma(0;0,0,0)$  components and  $\langle\gamma\rangle(0;0,0,0)$  ( $10^{-37}$  esu) values for **5** and **6** computed by TDHF method with 6-31G(*d*) basis set.

**Table 8:** Selected components of the frequency-dependent  $\alpha(-\omega;\omega)$  and absolute values of  $\langle\alpha\rangle(-\omega;\omega)$  ( $10^{-24}$  esu) at  $\omega = 0.04282$  a.u for **5** and **6** computed by TDHF method with 6-31G(*d*) basis set.

**Table 9:** Selected components of the frequency-dependent  $\beta(-2\omega;\omega,\omega)$  and  $\beta - V$  ( $10^{-30}$  esu) values at  $\omega = 0.04282$  a.u for **5** and **6** computed by TDHF method with 6-31G(*d*) basis set.

**Table 10:** Selected components of the frequency-dependent  $\gamma(-3\omega;\omega,\omega,\omega)$  and absolute values of  $\langle\gamma\rangle(-3\omega;\omega,\omega,\omega)$  ( $10^{-37}$  esu) at  $\omega = 0.04282$  a.u for **5** and **6** computed by TDHF method with 6-31G(*d*) basis set.

**Table 1:** Electronic parameters of **5** and **6**.

Compound	Absorption $\lambda_{\max}$ (nm) / $\epsilon$ ( $\times 10^5$ M $^{-1}$ cm $^{-1}$ )	$\lambda_{\text{onset}}$ (nm)	$E_{\text{gap}}$ (eV)	FWHM (nm)
<b>5</b>	395 (0.758)	481	2.578	75.0
<b>6</b>	339 (0.348), 417 (0.766)	493	2.515	78.5

**Table 4:** Calculated electric dipole moments,  $\mu$  (Debye) and dipole moment components for **5** and **6** using DFT method at B3LYP/6-31G(*d*) level.

Compound	$\mu_x$	$\mu_y$	$\mu_z$	$\mu$
<b>5</b>	0.000	0.000	-1.726	1.726
<b>6</b>	0.000	0.000	-0.814	0.814

**Table 9:** Selected components of the frequency-dependent  $\beta(-2\omega; \omega, \omega)$  and  $\beta - V$  ( $10^{-30}$  esu) values at  $\omega = 0.04282$  a.u for **5** and **6** computed by TDHF method with 6-31G(*d*) basis set.

Compound	$\beta_{xxx}$	$\beta_{yyy}$	$\beta_{zzz}$	$\beta_x$	$\beta_y$	$\beta_z$	$\beta - V$
<b>5</b>	0.0	0.0	1.5	0.0	0.0	52.6	52.6
<b>6</b>	0.0	0.0	1.8	0.0	0.0	85.9	85.9

**Table 5:** Selected components of the static  $\alpha(0;0)$  and  $\langle\alpha\rangle(0;0)$  ( $10^{-24}$  esu) values for **5** and **6** computed by DFT method at B3LYP/6-31G(*d*) level.

Compound	$\alpha_{xx}$	$\alpha_{yy}$	$\alpha_{zz}$	$\langle\alpha\rangle$
<b>5</b>	175.1	194.2	79.6	149.6
<b>6</b>	206.3	214.9	81.9	167.7

**Table 7:** All static  $\gamma(0;0,0,0)$  components and  $\langle\gamma\rangle(0;0,0,0)$  ( $10^{-37}$  esu) values for **5** and **6** computed by TDHF method with 6-31G(*d*) basis set.

Compound	$\gamma_{xxxx}$	$\gamma_{yyyy}$	$\gamma_{zzzz}$	$\gamma_{xxyy}$	$\gamma_{xxzz}$	$\gamma_{yyzz}$	$\langle\gamma\rangle$
<b>5</b>	1306.4	3254.9	29.4	576.8	62.6	317.3	1300.8
<b>6</b>	2007.3	5586.5	31.3	753.0	91.1	428.7	2034.1

**Table 10:** Selected components of the frequency-dependent  $\gamma(-3\omega; \omega, \omega, \omega)$  and absolute values of  $\langle \gamma \rangle(-3\omega; \omega, \omega, \omega)$  ( $10^{-37}$  esu) at  $\omega = 0.04282$  a.u for **5** and **6** computed by TDHF method with 6-31G(*d*) basis set.

Compound	$\gamma_{xxxx}$	$\gamma_{yyyy}$	$\gamma_{zzzz}$	$\gamma_{xxyy}$	$\gamma_{xxzz}$	$\gamma_{yyzz}$	$\langle \gamma \rangle$
<b>5</b>	3025.0	8268.0	74.4	1273.9	146.5	778.0	3126.8
<b>6</b>	4606.6	19711.4	116.2	2029.2	231.3	1502.6	6526.5

**Table 2:** Calculated first HOMO, LUMO and second HOMO-1, LUMO+1 frontier MO energies and  $E_g$  for **5** and **6** using DFT method at B3LYP/6-31G(*d*) level.

Compound	HOMO (eV)	LUMO (eV)	HOMO-1 (eV)	LUMO+1 (eV)	$E_g$ (eV)
<b>5</b>	-4.33	-1.68	-5.06	-1.24	2.65
<b>6</b>	-4.27	-1.67	-4.95	-1.39	2.60

**Table 3:** Calculated absorption wavelengths, oscillator strengths and major compositions in terms of MO contributions for **5** and **6**.

Compound	State	Calculated absorption $\lambda$ (nm)	Oscillator strength ( $f$ )	Major contribution
<b>5</b>	Excited state 1	620.5	0.0011	HOMO→LUMO
	Excited state 2	486.8	0.0800	HOMO-1→LUMO HOMO→LUMO+1
	Excited state 3	409.4	0.9150	HOMO-1→LUMO HOMO→LUMO+1 HOMO→LUMO+2
<b>6</b>	Excited state 1	631.0	0.0013	HOMO→LUMO
	Excited state 2	429.0	0.8008	HOMO-1→LUMO HOMO→LUMO+1
	Excited state 3	347.5	0.4104	HOMO→LUMO+2

**Table 6:** Selected components of the static  $\beta(0;0,0)$  and  $\beta_{\text{tot}}(0;0,0)$  ( $10^{-30}$  esu) values for **5** and **6** computed by DFT method at B3LYP/6-31G(*d*) level.

Compound	$\beta_x$	$\beta_y$	$\beta_z$	$\beta_{\text{tot}}$
<b>5</b>	0.0	0.0	41.3	41.3
<b>6</b>	0.0	0.0	66.5	66.5

**Table 8:** Selected components of the frequency-dependent  $\alpha(-\omega;\omega)$  and absolute values of  $\langle\alpha\rangle(-\omega;\omega)$  ( $10^{-24}$  esu) at  $\omega = 0.04282$  a.u for **5** and **6** computed by TDHF method with 6-31G(*d*) basis set.

Compound	$\alpha_{xx}$	$\alpha_{yy}$	$\alpha_{zz}$	$\langle\alpha\rangle$
<b>5</b>	103.8	116.3	41.2	87.1
<b>6</b>	126.8	126.6	41.9	98.5

Figure 1

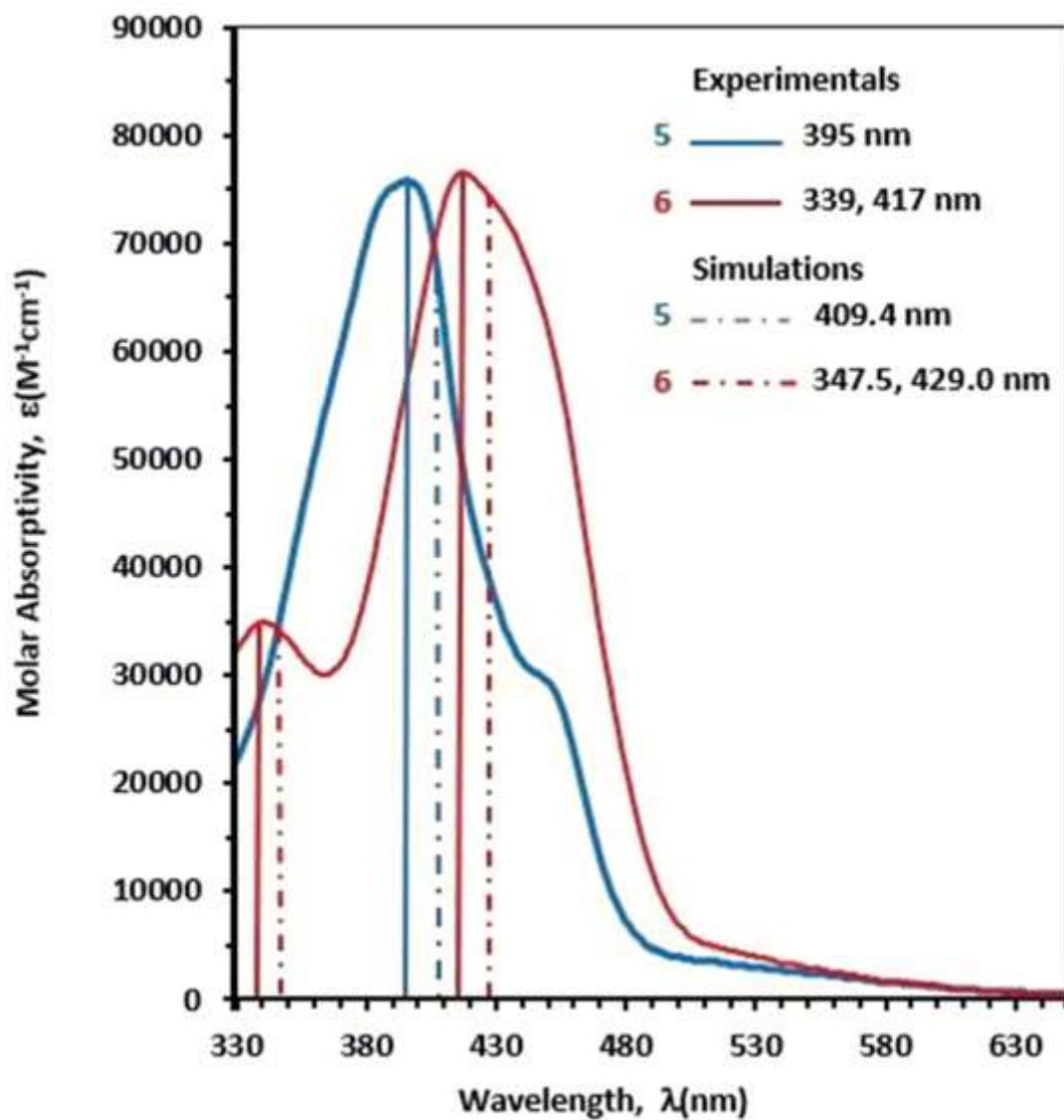


Figure 1

Figure 2

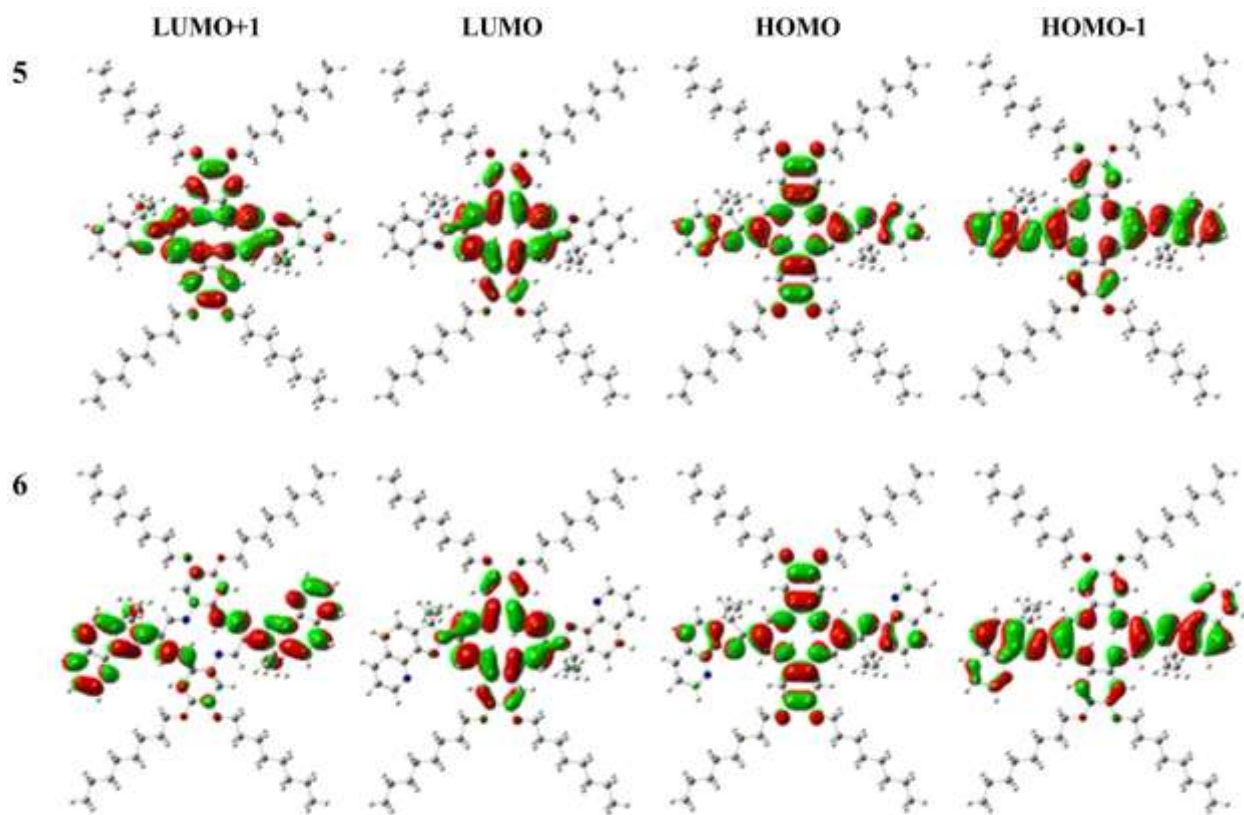
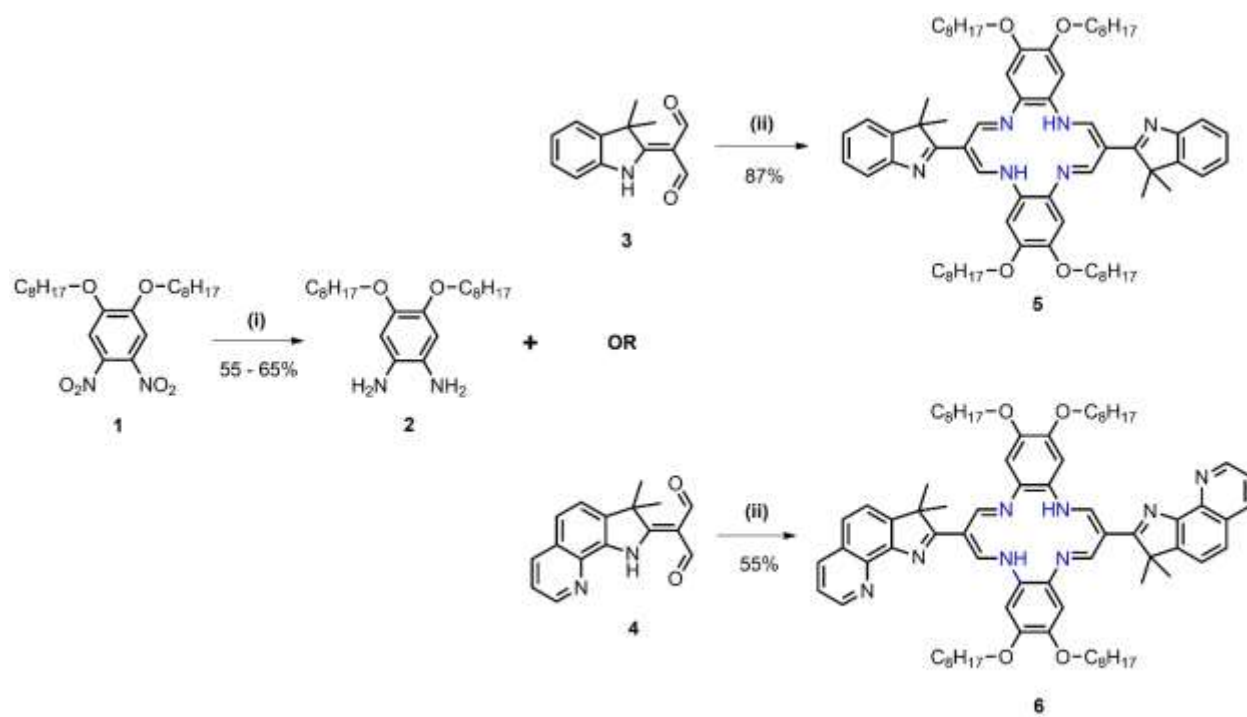


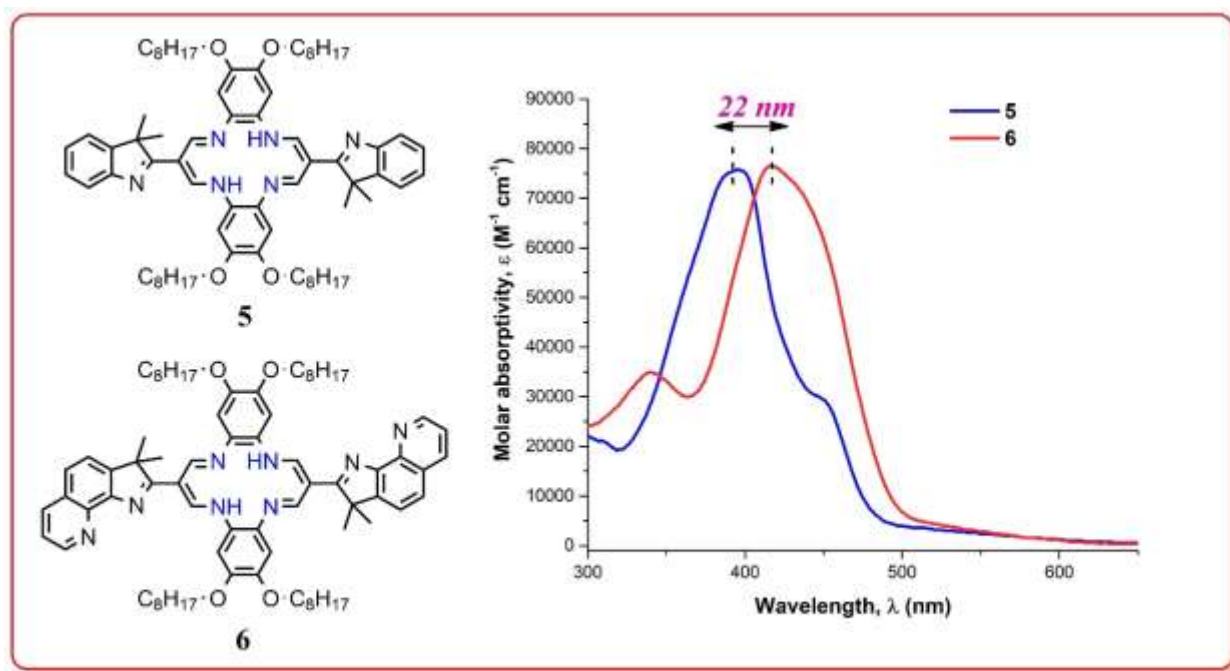
Figure 2

Scheme 1



Scheme 1

## Graphical Abstract



## Graphical Abstract